Eddies in Eastern Boundary Subtropical Upwelling Systems

X. Capet[1], F. Colas, and J.C. McWilliams

Institute of Geophysics and Planetary Physics, University of California at Los Angeles, Los Angeles, California, USA

P. Penven

Institut de Recherche pour le Developpement, UR097 ECO-UP, Centre IRD de Bretagne, Plouzané, France

P. Marchesiello

Institut de Recherche pour le Developpement, Noumea, New Caledonia

Over the last decade, mesoscale-resolving ocean models of eastern boundary upwelling systems (EBS) have helped improve our understanding of the functioning of EBS and, in particular, assess the role of eddy activity in these systems. We review the main achievements in this regard and highlight remaining issues and challenges. In EBS, eddy activity arises from baroclinic/barotropic instability of the inshore and also offshore currents. Mesoscale eddies play a significant (although not leading) role in shaping the EBS dynamical structure, both directly and through associated submesoscale activity (i.e., primarily frontal). They do so by modifying both momentum and tracer balances in ways that cannot simply be understood in terms of diffusion. The relative degree to which these assertions about eddy activity and eddy role apply to each of the four major EBS (Canary, Benguela, Peru–Chile, and California Current Systems) remains to be established. Besides resolving the eddies, benefits from EBS high-resolution modeling include the possibility of accounting for the fine-scale structures of the nearshore wind, a better representation of the Ekman-driven coastal divergence, and (at resolution $\mathcal{O}$ (1 km) or lower) inclusion of submesoscale (i.e., mainly frontal) processes. Recent numerical experiments suggest that accounting for these various processes in climate models, through resolution increase (possibly locally) or parameterization, would lead to significant basin-scale bias reduction. The mechanisms involved in upscaling from EBS toward the larger scale remain to be fully elucidated.

1. INTRODUCTION

Subtropical oceanic regions off the western coasts of America and Africa are generally referred to as eastern boundary systems (EBS) and share some important characteristics. The subtropical basin-scale circulation and thermohaline structure are characterized by a broad, slow gyre flow directed equatorward and a shallow thermocline. The atmos-

[1]Now at Instituto Oceanografico, University of São Paulo, Brazil.

Ocean Modeling in an Eddying Regime
Geophysical Monograph Series 177

10.1029/177GM10

pheric pressure patterns (highs offshore and lows inland) are conducive to alongshore and equatorward wind regimes and hence to coastal upwelling. Although these two dynamical components (the large-scale circulation and the coastal upwelling) can be considered in isolation, it really is their combination and interplay that lead to the observed oceanographic conditions in the Canary, Benguela, Peru-Chile, and California current systems (respectively denoted by CS, BS, PCS, and CCS). For example, thermocline shallowness is not a mere consequence of the coastal upwelling; on scales of 1,000 km or more, it is also understood in terms of Sverdrup theory, i.e., thermocline deepening toward the west (the direction of Rossby wave propagation). Exemplary features that further illustrate the interplay between the coastal and large-scale dynamics are the upwelling filaments that carry newly upwelled water from the coast to hundreds of kilometers offshore.

Although to different degrees and with significant time variability, EBS have high primary productivity that indirectly sustains intensive fishing activity (more than 20% of the global fish catch takes place within these narrow bands). This is perhaps the main reason why EBS received considerable attention early in the development of modern oceanography and are still a favored place for oceanographic research (e.g., AOSN, *Deep Sea Res.*, special issue; AESOP, http://www.mbari.org/MB2006/AESOP/mb2006-aesop-links.htm; and VOCALS, http://www.eol.ucar.edu/projects/vocals/). In particular, numerical models have been widely applied to these regions, initially for the purpose of understanding processes and increasingly for forecasting on timescales ranging from days to decades. Modeling progress has generally been slow, and we can suggest two explanations. First, eddies and other mesoscale (i.e., with horizontal scales larger than, but comparable to, the first baroclinic deformation radius R_d), or even submesoscale features (e.g., jets, filaments, or fronts that are characterized by at least one horizontal length scale less than R_d), are essential flow components for the dynamical and biogeochemical functioning of the system. In this regard, EBS are similar to many other oceanic regions where mesoscale turbulence is intense. Note, though, that some characteristics of EBS favor energetic submesoscale activity, especially close to shore [*Durski and Allen*, 2005; *Pedlosky*, 1978; *Barth*, 1994, section 5.1]. Therefore, even eddy-permitting primitive-equation models (i.e., with a couple of grid points to resolve R_d) have difficulty capturing EBS dynamics adequately within a few hundred kilometers of the shore.

Second, the validity of quasi-geostrophic theory breaks down almost by definition in EBS regions because the driving process, i.e., the coastal upwelling, leads to isopycnal outcropping and rather large Froude numbers. Therefore, quasi-geostrophic models have had limited success in reproducing EBS dynamics [*Pares-Sierra et al.*, 1993; *Ikeda and Emery*, 1984].

The aim of this chapter is threefold. In sections 2 and 3, we present some of the main results accumulated over the last decade by mesoscale-resolving EBS numerical studies. These studies have been made almost exclusively using regional models[1] because eddy-resolving global (or even basin-scale) numerical solutions have only become recently affordable. Global models will remain expensive for the years to come, and extensive sensitivity studies, such as those performed using regional models, are still beyond reach. Furthermore, the large-scale modeling community has generally neglected EBS regions because they are considered not of primary importance for the global circulation, as opposed to passage flows and western boundary currents, for example. As modeling errors in the latter regions are being reduced, those related to EBS are beginning to emerge. In section 4, we report on evidence that EBS regions, indeed, exert upscaling effects on the dynamics of their respective oceanic basins. Some important difficulties that hinder further progress in EBS mesoscale modeling are outlined in section 5, and concluding remarks are offered in section 6.

2. GENERATION OF MESOSCALE ACTIVITY IN EBS

Taken as a rough measure of mesoscale activity, the surface eddy kinetic energy (EKE)[2] in EBS is relatively low (lower than 250 $cm^2\ s^{-2}$, Plate 1) compared to the most active regions of the world ocean [*Ducet et al.*, 2000]. However, the EBS EKE stands out in the otherwise quiescent subtropical eastern Pacific on global maps of EKE [Plate 8 in *Ducet*

Plate 1. (Opposite) Measured EKE ($cm^2\ s^{-2}$) and sea-surface height (SSH; with 6-cm contour interval; open lines) in the four EBS. SSH contours are also the streamlines for the surface geostrophic current whose direction is indicated by small arrows. EKE is computed from the improved DUACS SSH product for the period 2001–2006 [*Pascual et al.*, 2006]. SSH is computed from Rio05 [*Rio and Hernandez*, 2004] that combines altimetry and gravimetry satellite measurements together with temperature and salinity in situ data (World Ocean Atlas, *Boyer and Levitus* [1998]). Note the good correspondence between high EKE and tight SSH contours at the Azores front, off Central Chile, and off North America.

Plate 2. (Opposite) Top: Same as Plate 1 for a reduced domain. Bottom: EKE and SSH contours from ROMS solutions at 5 km. The EKE is computed using low-pass filtered (6-day averaging and Gaussian spatial filter with 30-km half-width) geostrophic velocities. *Color bars* and SSH intervals are the same for models and observations.

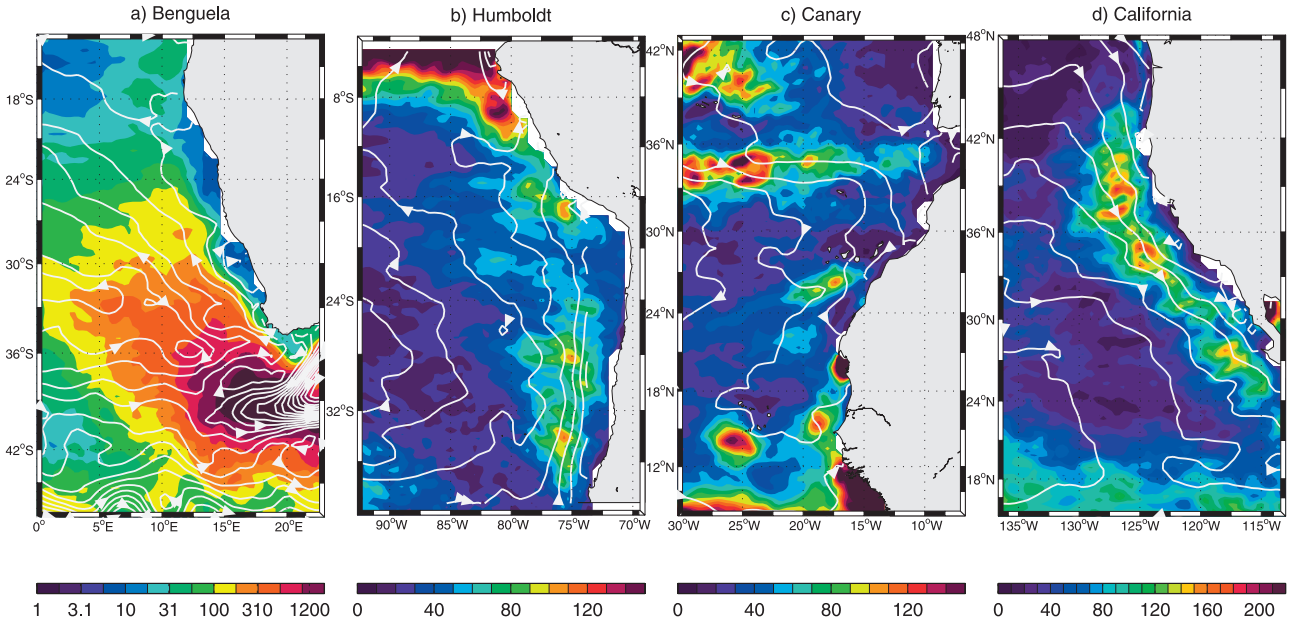

Plate 1.

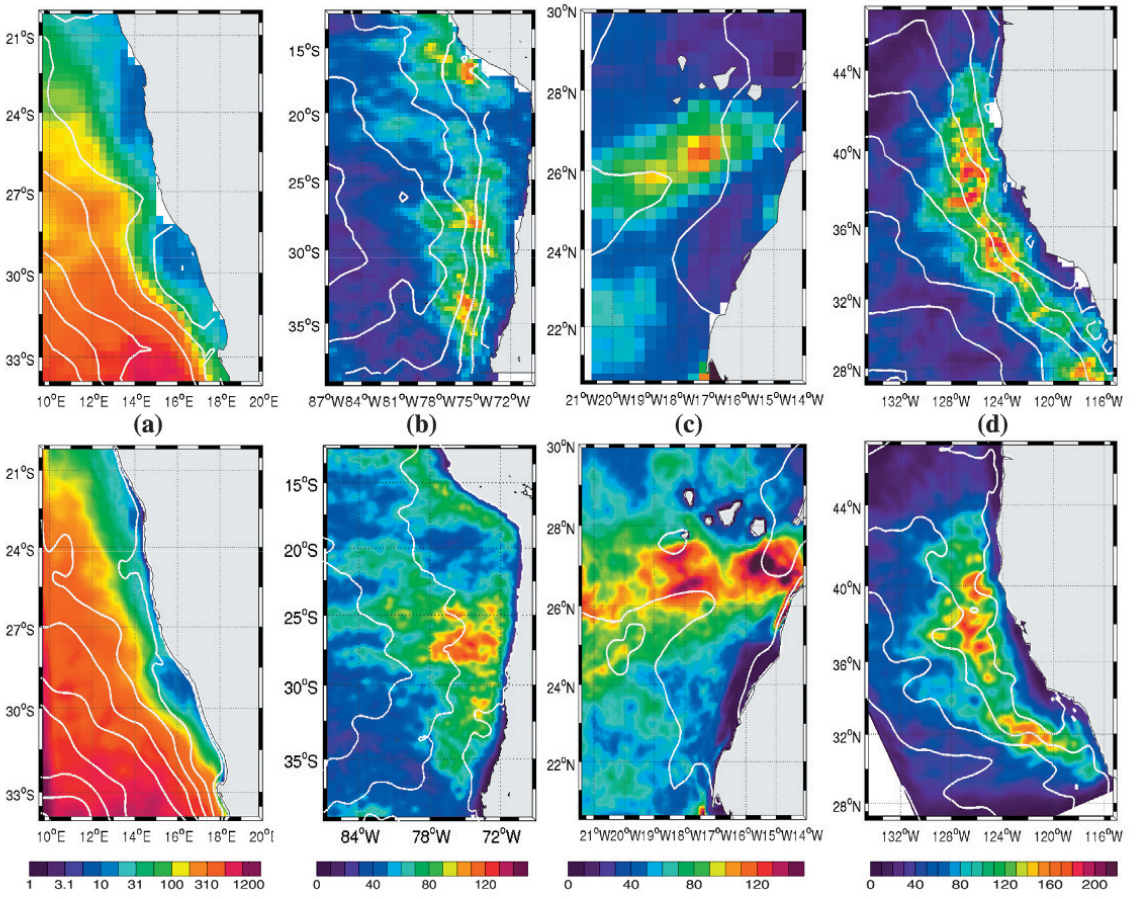

Plate 2.

et al., 2000]. This is less true in the subtropical eastern Atlantic because mesoscale activity in the CS is weaker than in the other systems for reasons discussed by *Marchesiello and Estrade* [2008] and because the Agulhas Rings overshadow all other sources of mesoscale activity in the southeastern Atlantic.

2.1. Coastal Versus Offshore Generation

We start by reviewing the surface EKE sources in EBS. Early on, idealized studies [*Ikeda et al.*, 1984; *Ikeda and Emery*, 1984] suggested coastal current instabilities for EKE generation, as opposed to wind variability. One of the major achievements of eddy-resolving models in the 1990s is the widely accepted demonstration that mesoscale variability in EBS arises in large part from the instability of coastal currents [*Batteen*, 1997; *Leth and Middleton*, 2004]. This is seemingly at odds with EKE maps derived from altimetric sea-level anomalies that tend to show EKE local minima in a band 100 to 300 km nearshore (Plate 1). EKE coastal minima are found off central Chile, Morocco and Mauritania, and central California. Along the coast of South Africa, EKE levels are also weak, but the situation is peculiar because the offshore region is in the path of the Agulhas Rings. Note that relatively high coastal values indicative of nearshore EKE sources can also be found, e.g., around 36–38°S and 30°S along the Chilean coast; 12–15°N along the coast of Senegal (the high values south of Cape Blanc at 19°N are for the Arguin Bank, a large expanse of water less than 20 m deep where wind-driven variability is probably essential); 38–42°N along the North American West Coast; and around 30°S off South Africa. These regions correspond to well-known upwelling centers.

There are several explanations for the EKE relative minima nearshore. The obvious one is that the sea-surface height (SSH) product, which EKE is derived from, is oblivious to non-geostrophic currents and, more generally, to eddy activity associated with wavelengths smaller than 0.5° [*Ducet et al.*, 2000]. As eddy activity tends to be at small scales nearshore and undergoes an inverse cascade while moving westward, it is progressively more detectable by the altimeter, hence the offshore maximum. A more subtle reason is that mean offshore currents can significantly contribute to eddy variability, however weak and elusive. This might be anticipated on the theoretical grounds for destabilization of meridional currents [*Pedlosky*, 1987; *Spall*, 2000].[3] In the framework of an eastern boundary system, this is confirmed by *Marchesiello et al.* [2003] who simulate a realistic CCS (i.e., the coastal and large-scale circulation, the termination of the West-Wind Drift, and the offshore California Current) and show that eddy activity is due to the intrinsic variability of the system as a whole, with significant EKE sources as far as 500 km off the California-Oregon coast. More specifically, in the offshore region, the main source of energy for eddies is baroclinic conversion (from mean potential to eddy kinetic energy), whereas nearshore, it is more evenly split between baroclinic and barotropic (from mean to eddy kinetic energy) conversion. Thus, EKE patterns may not reflect only advection and propagation of mesoscale structures generated nearshore [*Chaigneau and Pizarro*, 2005; *Hormazabal et al.*, 2004]. The good correspondence between large EKE and intense mean flow in several places in Plate 1 further supports this view.[4] In practice, trying to distinguish eddy activity generated by offshore versus coastal currents may not be very meaningful in this turbulent equilibrium regime: coastal and offshore currents and eddies strongly interact with each other.

Numerical models can now be run at horizontal and vertical resolutions that permit a good representation of eddies in the ocean. However, this does not guarantee a correct EKE field. In fact, given the complexity of EKE generation, surface EKE comparison between a model and data is a stringent test of the upper-oceanic circulation. Using adequate forcing (section 5.2), regional models, such as regional ocean modeling system (ROMS), are able to reproduce general surface EKE patterns with some localized discrepancies and possibly large-scale magnitude differences [e.g., in the southern PCS and CS in particular, EKE is 20 to 30% too high, and in the northern PCS model, EKE is a bit low for reasons discussed by *Penven et al.* 2005]. More rigorous comparisons will be required where numerical solutions are processed in the same way as altimetric observations to be entirely conclusive (in Plate 2, numerical solution EKEs were computed from low-pass filtered 2D sea surface elevations to limit inconsistencies in the estimates).

Although we focus on surface eddy activity, some eddies are subsurface-intensified with little or no hydrographic signature at the surface [*Cornuelle et al.*, 2000]. The general generation mechanism is instability of the nearshore undercurrents [with subsequent insemination of the offshore domain, *Brink et al.* 2000], although offshore generation cannot be ruled out [for the US West Coast (USWC), see *Collins et al.*, 2004]. Numerical models produce subsurface-intensified eddies [*Marchesiello et al.*, 2003], and insofar as their nearshore currents are realistic, they are useful in complementing the generally sparse observational information on the generation, structure, and effects of such eddies.

2.2. Seasonality and Low-Frequency Variability

The average picture described in the previous section is incomplete because mesoscale activity in EBS exhibits considerable variability. A seasonal cycle arises from the wind and heat flux cycles. In the CCS, northern CS, and southern

PCS, coastal surface EKE generation is most pronounced in spring when the upwelling favorable winds pick up, and the current system is concentrated nearshore. The location of the maximum surface EKE then migrates offshore with a significant attenuation over 300 to 500 km. In winter, the surface EKE is relatively weak without any clear maximum. Closer to the equator (northern PCS and BS, southern CS, and CCS), the upwelling is more persistent with a reversed (maximum in fall and winter off Peru) or no EKE seasonal cycle and no clear offshore migration of the EKE signal. In the CCS, the migration and attenuation are both observed in the data [*Kelly et al.*, 1998] and captured in numerical models [*Haney et al.*, 2001; *Marchesiello et al.*, 2003]. These models have played a key role in explaining the underlying dynamics, i.e., barotropization and subduction [*Haney et al.*, 2001] as opposed to an eddy-damping mechanism.

Mesoscale activity can also be modulated on interannual timescales. In the Pacific, the modulation arises primarily from the nearshore circulation changes caused by El Niño Southern Oscillation (ENSO). During El Niño events, currents are intensified poleward. Their destabilization leads to anticyclonic eddy formation especially in the lee of the major capes and headlands, as observed along Peru-Chile and the Mexican, USA, and Canadian West Coasts [*Strub and James*, 2002]. Using an eddy-resolving layered model, *Murray et al.* [2001] demonstrate that anticyclonic eddies shed by the baroclinically unstable coastal currents in the Gulf of Alaska largely control the vorticity budget over the entire region. Similar anticyclones are formed during the 1997–1998 El Niño in a PCS ROMS solution run with realistic forcing (ERS winds and oceanic boundary conditions are derived from a global POP solution; see Colas et al., 1997–1998 El Niño off Peru: A numerical study, submitted to *Progress in Oceanography*, 2007, hereinafter referred to as Colas et al., submitted manuscript, 2007). Although quantitative analyses are needed, these eddies evidently play a role in advecting anomalous water masses and tracer properties (vorticity, heat, and salt) brought from the equatorial region. In the CS, the inter-annual variability is essentially locally forced by the wind variability, as shown by *Roy and Reason* [2001], with the sea-surface temperature (SST) correlated to the ENSO signal with a 4-month phase lag. In the BS, major intrusions of warm saline water of equatorial origin can reach as far as 25°S and are associated with positive coastal sea level anomalies and an increased poleward current. This phenomenon is related to wind anomalies in the western and central Atlantic and is called the Benguela Niño by analogy with its Pacific counterpart [*Shannon et al.*, 1986; *Gammelsrod et al.*, 1998; *Florenchie et al.*, 2004]. The impact of basin-scale interannual variability in the CS and BS has not received significant numerical (or observational) attention.

3. EFFECTS OF THE MESOSCALE IN EBS

3.1. Tracer and Momentum Eddy Fluxes

EBS regions do not have especially large eddy-rectification effects, ignoring the southern part of the Benguela where most of the eddy activity is in fact that of the Agulhas Current that is diverted western boundary current. Bolus velocities[5] are rather small in EBS [*Bryan et al.*, 1999] (but note that they are only computed for density classes that never outcrop at a given location). This should be no surprise considering the fact that isopycnal thickness is quite uniform and the isopycnals rather flat except at the very nearshore (Plate 3); again, this does not apply to the southern Benguela. However, the mean circulation is also weak so that eddy fluxes can potentially exert some influence on EBS dynamical balances [*Marchesiello et al.*, 2003; *Leth and Middleton*, 2004]. Although observations lead to reliable estimates of eddy activity in the ocean (e.g., altimetry outside the nearshore region), they arguably lack spatial and temporal coverage over long enough timescales to allow for comprehensive estimates of eddy effects (fluxes of tracer and momentum and, most importantly, their divergence; *Colbo and Weller*, 2008). Numerical models are a well-suited framework to address these issues provided that they possess a reasonable degree of realism. Depth-integrated vorticity and heat budgets are calculated in *Marchesiello et al.* [2003] [see also *Leth and Middleton*, 2004]. In the CCS, eddy fluxes were found to modify the Sverdrup relation by inducing poleward flow within 150 km from shore and equatorward flow between 150 and 300 km from shore. Comparable budget analyses are lacking for the other systems, but the mechanism is presumably generic. A possible exception would be the northern part of the PCS where the mean offshore circulation is directed poleward rather than equatorward as in all other systems.

Using mesoscale-resolving regional configurations, Capet et al. (Upwelling systems heat balance: Role of the eddies, submitted to *Journal of Marine Research*; hereinafter referred to as Capet et al., submitted manuscript, 2007) examine the upper-oceanic heat budget (1) because of its importance in the coupled atmosphere–ocean system and in particular in the atmospheric boundary layer (section 4).

$$\int_{z_0}^{\zeta} \partial_t \overline{T} dz = -\int_{z_0}^{\zeta} \nabla \cdot \overline{\mathbf{u}T} dz + Q_{as} - \overline{\kappa \partial_z T}|_{z_0}$$

$$T_c = A + Q_{as} + D \tag{1}$$

In (1), $\mathbf{u}$ is the 3D velocity, T the potential temperature, ζ the sea surface elevation, κ the vertical subgrid-scale

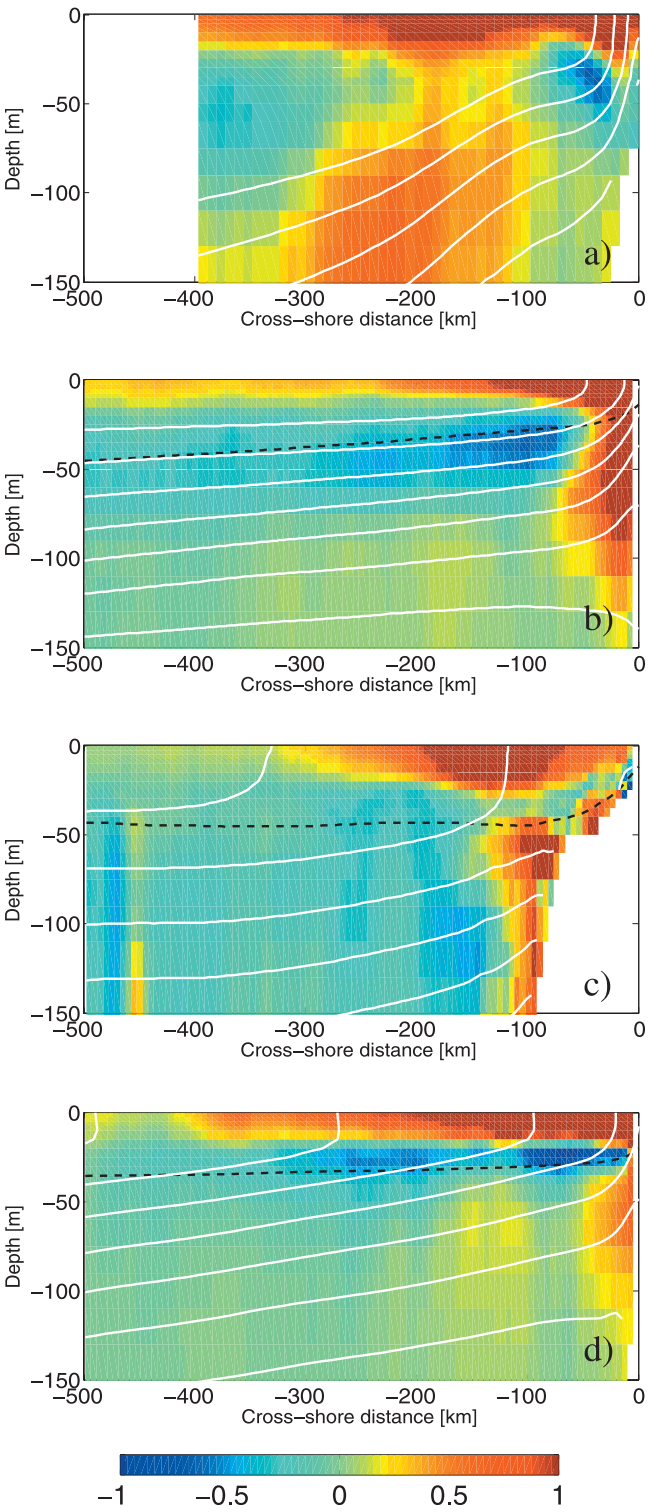

Plate 3. Vertical sections of annual-mean eddy heat flux divergence (W m^{-3}) for BS, PCS, CS, and CCS (top to bottom) ROMS solutions. Alongshore averaging is done between, respectively, 25–33°S, 15–25°S, 22–26°N, and 35–43°N. The solid dashed line indicates the mean depth of the surface boundary layer. Open lines represent isotherms (at 1° intervals) that is approximately isopycnals because salinity effects are minor.

diffusivity, and Q_{as} the ocean–atmosphere heat flux including both interface fluxes and penetrating shortwave radiation. $\overline{\cdot}$ represents a time-averaging operator. By integrating deep enough (typically $z_0 = 100$ m) and long enough (5 years or more), T_c and D are negligible in EBS. The advection term is further decomposed into mean and eddy contributions presented along with their sum in Plate 4 for the PCS. The mean and eddy terms exhibit significant spatial variability that is absent from their sum. This might be attributed in part to insufficient averaging, especially offshore where convergence as a function of the averaging period seems to take place, albeit slowly, a point that further underlines the difficulty in analyzing heat balances from observations with limited temporal extent.

Nearshore, where spatial variability is most conspicuous, standing eddies play a prominent role in shaping robust structures that have also been observed in nature by their imprint on velocity and temperature (Centurioni, et al., Permanent meanders in the California Current System and comparison of near-surface observations with OGCM solutions, submitted to *Journal of Physical Oceanography*, 2007). This is especially the case in the CCS where standing eddies produce alternating strips of warming and cooling with a magnitude more than 50 W m^{-2} (not shown).

In all systems, the primary balance is between mean advection and atmospheric fluxes, except within roughly 50 to 100 km from shore where eddy fluxes provide a warming contribution that significantly counteracts cooling by the mean advection (in the CS and parts of the BS, the band of large positive eddy flux divergence is displaced farther offshore, but remains centered over the upper-slope and shelf-break where the upwelling takes place).

Farther offshore, the eddy flux divergence modulates the heat budget with clear signs of cooling over extended regions: off southern Peru (Plate 4), northern California-Oregon, Mauritania-Senegal, and in the Southern California Bight. These regions share the particularity of having a temperature maximum a few hundred kilometers from the coast. As a consequence, mean cross-shore advection in the boundary layer (mainly Ekman) turns into a warming term at some distance away from the coast. This leaves just the eddies to provide the cooling necessary to balance (1). In our solutions, we find an eddy cooling equivalent to −30 W m^{-2}. We emphasize that all these regions are important stratus cloud formation sites for which accurate heat budgets are greatly needed.

3.2. (Sub-)Mesoscale Vertical Fluxes and Subduction

Plate 3 shows vertical sections of eddy heat flux divergence averaged alongshore in the different systems. In accordance with the description in section 3.1, eddy activity in the CCS and PCS tends to cool the offshore domain when averaged over the upper hundred meters, but it also strongly warms the upper half of the boundary layer. The latter effect (and part of the cooling underneath) arises from the vertical component of the eddy heat flux. Ageostrophic secondary circulations that accompany frontogenesis [*Hoskins*, 1982], even at moderately high resolution, act to restratify the near-surface ocean [*Lapeyre et al.*, 2007; *Capet et al.*, 2008b]. The strain induced by the mesoscale eddy field is the key to this process, but the strength of the secondary circulations, and hence the restratification tendency, strongly increases with horizontal resolution, even below 1 km. Around such resolution, the emergence of a baroclinic submesoscale instability can be observed [*Capet et al.*, 2008b] and may contribute to the increased vertical fluxes. Other types of instability may be present as well [*Haine and Marshall*, 1998; *Boccaletti et al.*, 2007].

Traditionally, nearshore upwelled waters are viewed as remaining in the boundary layer where they are carried away by the Ekman flow. During this journey, they are progressively warmed by mixing with surface waters of offshore origin and by atmospheric heat flux. This description, sketched in Plate 5, is consistent with the circulation in oceanic general circulation models (OGCMs) and even mesoscale-resolving EBS models in which restratification is primarily confined to the boundary layer where it is counteracted by mixing arising from wind-induced turbulence. However, at resolutions of around 1 km or below, there are occurrences of subduction events that reach well below the boundary layer (Plate 6) at the edges of mesoscale eddies in the vicinity of surface density fronts. These aspects have been investigated in a submesoscale-resolving (750-m grid size) configuration for an idealized CCS and confirm observational evidence of widespread subduction at depths greater than 100 m [*Kosro et al.*, 1991; *Bograd and Mantyla*, 2005]. Thus, a new element is currently being added to our conceptual view of offshore Ekman transport in EBS. A substantial fraction of newly upwelled water is subducted on its way seaward, while an equivalent amount of upper thermocline water is drawn into the boundary layer (the colored arrows in Plate 5). The importance of subduction within EBS is still unclear, but this process has serious implications for the upper-oceanic heat balance (Capet et al., submitted manuscript, 2007), the transfer of organic material between the euphotic zone and the oceanic interior[6] and possibly EBS thermocline ventilation in general [*Bograd and Mantyla*, 2005]. We expect multiyear, submesoscale-resolving numerical solutions to play a major role in elucidating these questions and providing new insights to be incorporated into OGCMs by means of parameterizations (Fox-Kemper and Ferrari, Parameterization of

mixed layer eddies. II: Prognosis and impact, submitted to *Journal of Physical Oceanography*, 2007).

3.3. Mesoscale Activity and Meridional Contrasts in EBS

In EBS, the main frontal feature arises from thermohaline contrasts between nearshore freshly upwelled waters and offshore waters. On average, a front thus runs roughly parallel to the coastline. Other fronts are also present in EBS that stem from meridional gradients in water mass properties; such fronts have a roughly zonal orientation. This is the case for the Benguela-Angola front (at ≈15°S) that separates the Benguela cold waters from the much warmer and more saline northern waters; the Cape Verde front off Mauritania-Senegal and the Ensenada front off Baja California (see Plate 7). Another example is the front between equatorial (25°C and warmer) and subtropical waters (24°C and colder) that develops during El Niño off Peru (Plate 7). Note that this latter front has not been documented by in situ measurements. Model solutions suggest that these fronts are unstable (notice the meanders, filaments, and streamers in the vicinity of the fronts in Plate 7). The instabilities might be key in controlling the cross-front exchange of tracers on a regional scale and, consequently, the water mass that is being upwelled either along the Peruvian coast during El Niño (Colas et al., submitted manuscript, 2007) or along Mauritania-Senegal with some seasonal changes [*Perez-Rodriguez et al.*, 2001]. Further insight into the interplay between the coastal upwelling and such regional fronts would be useful.

4. UPSCALING EFFECTS ON EQUATORIAL CLIMATE

Recent studies indicate that EBS dynamics have nontrivial remote effects and, in particular, exert some influence over the equatorial regions. Using a non-eddy-resolving climate model, *Large and Danabasoglu* [2006] perform sensitivity experiments to evaluate the impact of the temperature warm bias that develops in such coarse coupled models. They compare a baseline solution with a solution that only differs by the fact that temperature within the EBS regions (one or several at a time) is heavily restored toward climatological values. The solutions with restoring exhibit significant improvements of their SST and, subsequently, precipitation patterns in the Pacific and Atlantic equatorial regions. The largest bias reduction is related to the PCS and BS. The impact of the CCS restoring is weak on near-surface properties, but it leads to a 1°–3°C subsurface temperature bias reduction across the entire Pacific between roughly 5°N and 15°N. Atmospheric connections from the EBS toward the equator—thought to occur by locally influencing the extensive stratus cloud deck—might at least partially explain these results. However, subsurface sensitivities suggest the existence of oceanic connections from the EBS toward the oceanic interior (*Large and Danabasoglu* [2006]; see also the analysis of an Atlantic reduced-gravity model by *Lazar et al*. [2002]). The sensitivity experiments presented in Section 5 suggest that eddy-resolving oceanic solutions forced by fine-scale wind fields (or coupled to a high-resolution atmospheric model) will be required to correct equatorial biases in OGCMs without resorting to numerical tricks such as the restoring by *Large and Danabasoglu* [2006].

EBS are also the place where long baroclinic Rossby waves are generated through coastally trapped wave leakage [*Philander and Yoon*, 1982]. Thus, coastal disturbances are transferred thousands of kilometers into the oceanic interior [*White et al.*, 1990; *Vega et al.*, 2003] with consequences that are as yet unclear. Again, the length scale of the processes in play (the baroclinic deformation radii for the cross-shore extension of the coastal trapped waves) implies that mesoscale-resolving oceanic models are needed to assess this issue. Note that another important generation mechanism for long baroclinic Rossby waves in EBS that is wind stress curl [*White and Saur*, 1981], is probably adequately represented in non-eddy-resolving models.

5. MODELING SUBTLETIES

5.1. Resolution Sensitivity

A benefit from high-resolution EBS simulations is better representation of the coastal divergence implied by the Ekman transport. It has been known for some time that mixing processes control the upwelling width, which becomes much less than the offshore deformation radius [*Pedlosky*, 1978], except when the upwelling occurs in regions with wide shelves (because bottom friction is significant over a wide nearshore strip; *Mitchum and Clarke*, [1986]; Estrade et al., Cross-shelf structure of coastal upwelling: A two dimensional expansion of Ekman's theory and a mechanism for innershelf upwelling shut down, submitted to *Journal of Physical Oceanography*, 2007, hereinafter referred to as Estrade at al., submitted manuscript. 2007). This makes upwelling in regions with narrow shelves (e.g., off central California and northern central Chile) very sensitive to horizontal resolution, down to scales hardly attainable with regional models, let alone global ones.[7] As an illustration, we show the summer-mean vertical velocity and temperature cross-sections at different resolutions (Plate 8 for an idealized CCS; *Capet et al.* [2008a]). Heat fluxes are adjusted with a restoring term that is only partly justified on physical grounds [*Barnier et al.*, 1995] so that the long-term impact

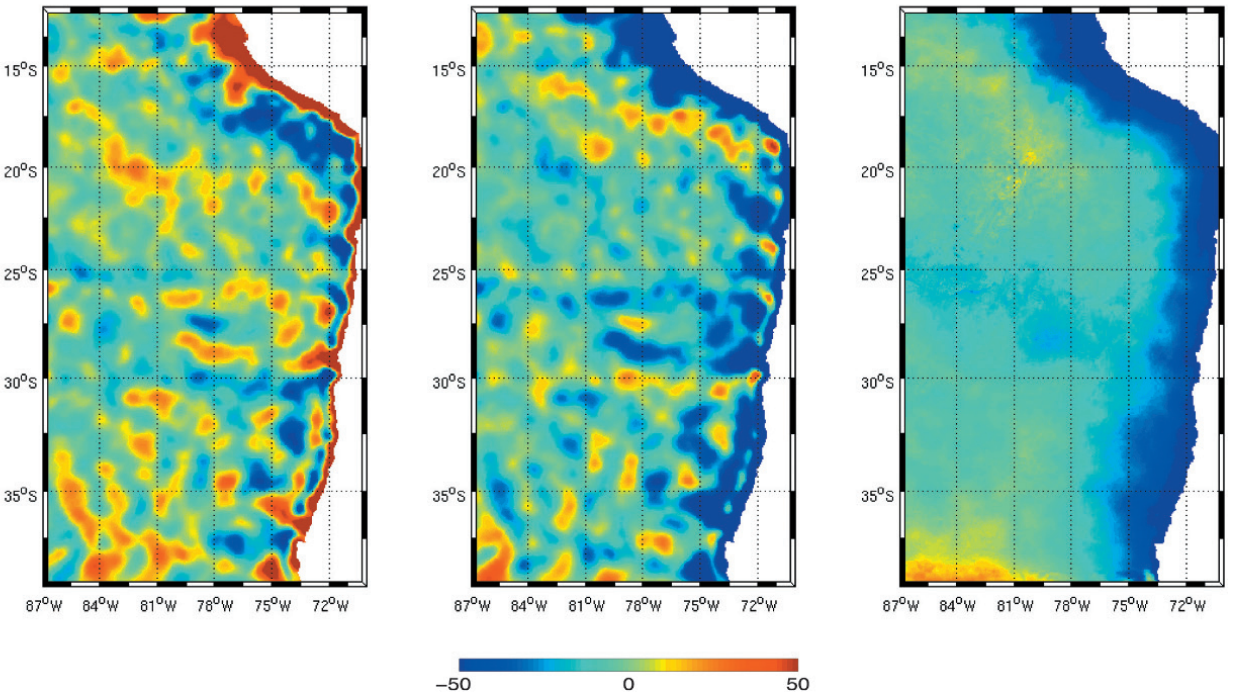

Plate 4. Annual average of vertically integrated (0- to 100-m depth) eddy (left), mean (center), and total (right) heat divergence (W m^{-2}) for a 9-year PCS ROMS solution. Maps of heat flux from the ocean to the atmosphere (i.e., positive upward) are indistinguishable from the panel for total heat flux.

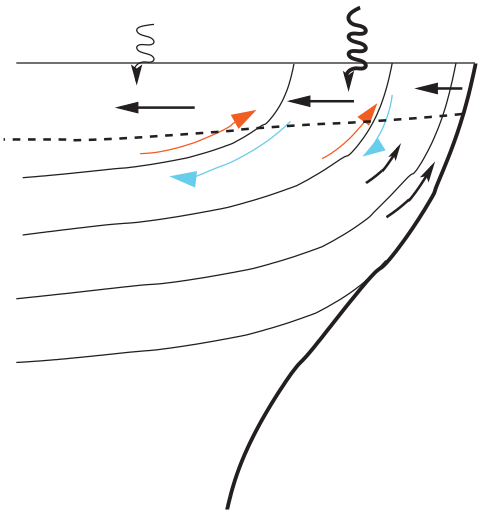

Plate 5. 2D schematic of coastal upwelling processes. Zigzag arrows represent atmospheric heat fluxes. The mixed layer base is delineated by a solid dashed line. Solid arrows indicate mean upwelling and Ekman transport, and the blue and red curved arrows indicate eddy fluxes, mostly along isopycnal surfaces. In the real 3D ocean, the favored locations for subduction or uplifting are related to the instantaneous positions of isopycnal surfaces as in Plate 6 (instead of the mean positions as suggested in this sketch).

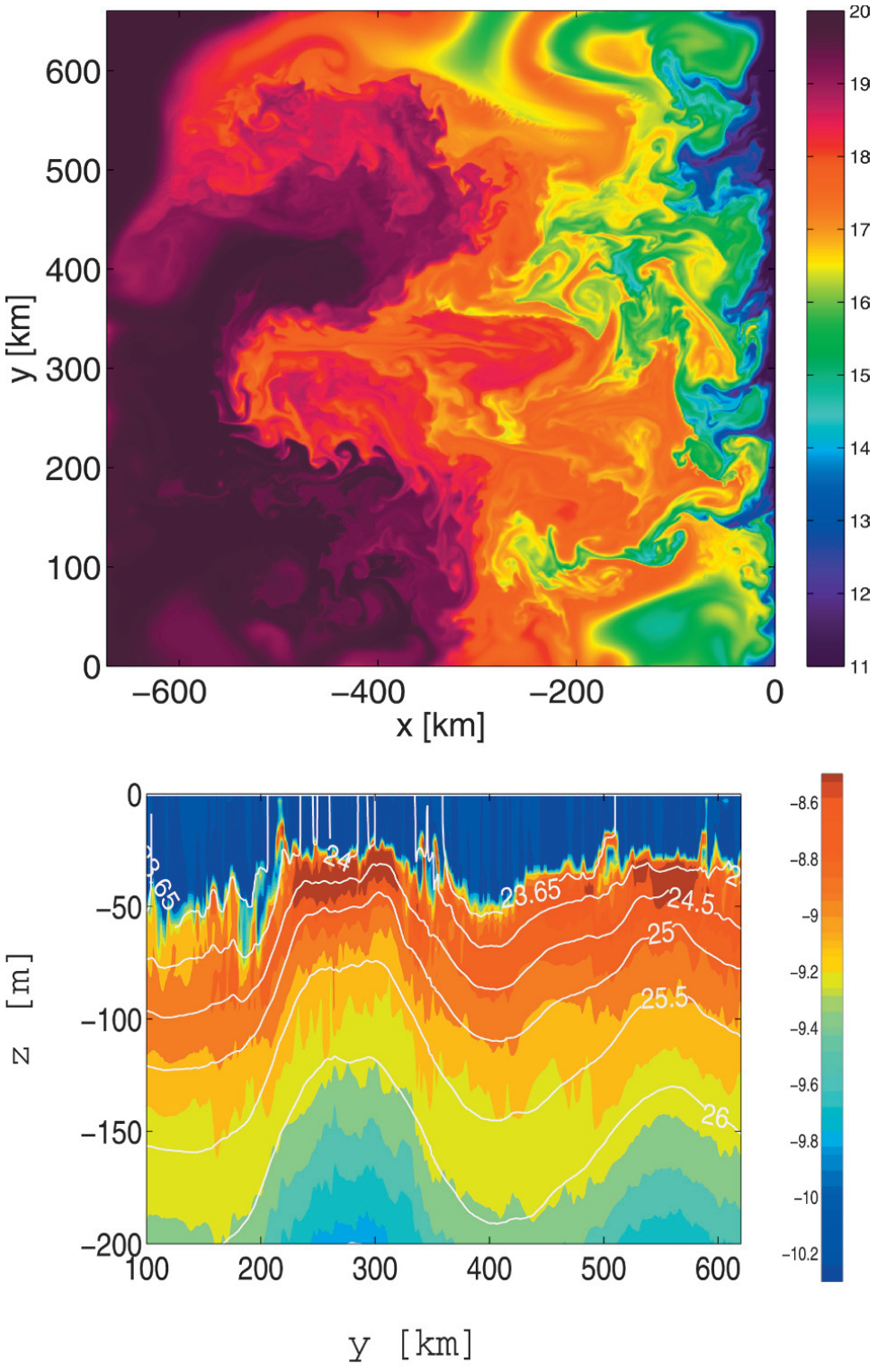

Plate 6. Top: instantaneous SST in an idealized CCS configuration (flat bottom; straight coastline on the right-hand side of the domain; constant upwelling favorable winds) [*Capet et al.*, 2007a]. Bottom: Ertel potential vorticity (PV, in color) and isopycnals (white contours) along the vertical section at $x = -400$ km. The region of low PV near the surface roughly delineates the boundary layer, with an abrupt transition to highly stratified waters (in red, the upper thermocline). Numerous intrusions between low and high PV waters can be seen. They generally coincide with the strongest density (or temperature) fronts at the edges of the main mesoscale structures.

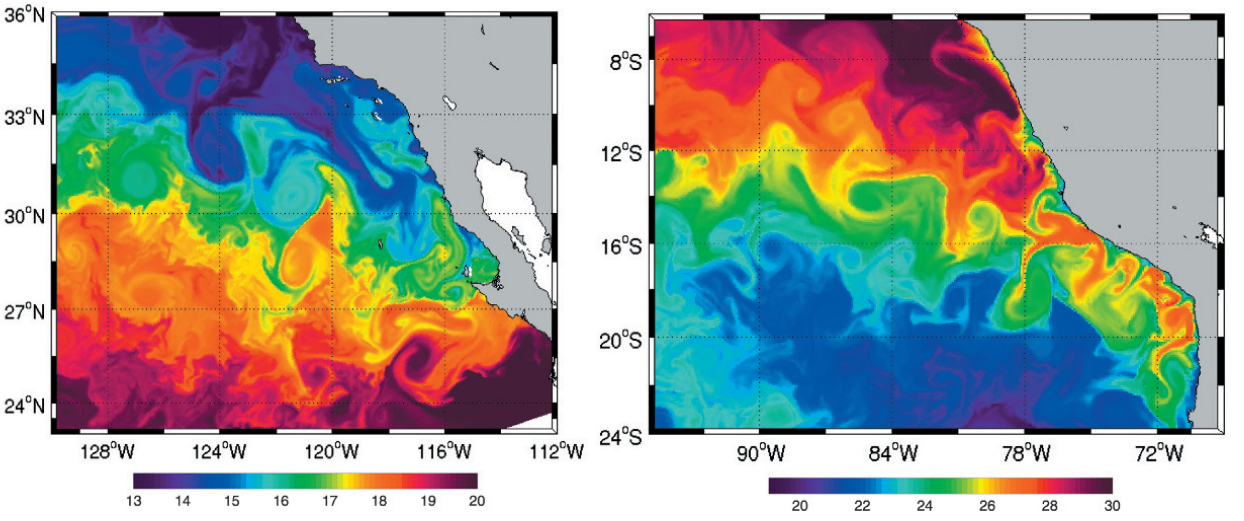

Plate 7. ROMS instantaneous potential temperature at 5 m. Left: during a climatological January off Southern California–Mexico; the unstable behavior of the Ensenada front is revealed by eddies and filaments. Right: in January 1998 shortly after the second major 1997–1998 El Niño pulse; a front separating equatorial from subtropical waters is noticeable as are its accompanying eddies, filaments, and streamers.

of resolution on the upper-oceanic temperature is uncertain. Nonetheless, the nearshore temperatures are almost two degrees colder at 750-m resolution than at 12 km. This difference is related to a tenfold increase in nearshore maximum vertical velocities that reach 50 m/day at the higher resolution, while the vertical flux of water remains roughly constant (because the same Ekman coastal divergence needs to be balanced). This is an important reason for the EBS warm bias present in non-eddy-resolving OGCMs.

5.2. Small Scales in Coastal Winds

It is common that some spatial and temporal uncertainties about atmospheric forcings exist, as analyzed in atmospheric data assimilation models and as simulated with coupled atmosphere-ocean models. The uncertainty is greatest near the shoreline because this is where the wind varies most rapidly and also because measuring or simulating nearshore winds is generally more challenging. QuikSCAT observations are sensitive to land contamination; spectral models such as NCEP suffer Gibbs phenomena nearshore when mountain ranges are present close to the coast that is virtually everywhere along eastern boundaries; nonspectral models still have issues handling the land-ocean transition. The degree to which the uncertainty in the forcing fields affects the oceanic solutions is an important issue. As already noted in section 2.1, upwelling system dynamics can be statistically well simulated without having to include synoptic and intra-seasonal wind fluctuations. In other words, rectification effects due to responses to the high frequencies in the wind are modest. On the other hand, sensitivity studies have demonstrated that mesoscale spatial variability of the nearshore wind has a large impact on upwelling systems. First, expansion fans [*Winant et al.*, 1988; *Enriquez and Friehe*, 1995; *Garreaud and Muñoz*, 2005], in conjunction with topographic irregularities, help the upwelling jet to separate away from the coast [*Castelao and Barth*, 2007] and subsequently generate standing meanders with scales of hundreds of kilometers. The mean nearshore wind profile is also important, and it can be understood in terms of the competition between coastal divergence and Ekman pumping. The occurrence of nearshore wind drop-off (i.e., a tendency for weaker winds toward the shore) favors upward Ekman pumping in a band somewhat distant from the coastline, while stronger nearshore winds (i.e., smaller or no drop-off) favor intense coastal upwelling. In the linear model of *Fennel and Laas* [2006], the outcome of this competition is sensitive to bottom friction. In realistic simulations off Central California and in the Southern California Bight, *Capet et al.* [2004] find that winds with limited drop-off lead to more upwelling, although the uplifting of particles due to Ekman pumping reaches deeper. The cross-shore wind profile close to shore also plays an important role in determining the alongshore current structure [*Marchesiello et al.*, 2003]. Equatorward winds at the coast force a surface equatorward jet and poleward undercurrent. The depth-averaged poleward currents are related to positive wind curl through Sverdrup balance with some modulation by the Reynolds stress (section 3.1). Large positive wind curl and weak coastal wind favor poleward currents and vice versa. The combination of these effects has important consequences on the system instability and on its resulting mesoscale activity.

To illustrate this, we compare the CCS solution presented in Plates 2d and 3d with that forced by NCEP winds (Plates 9 and 10). The winds for these two solutions differ mainly by the length scale they decrease by toward the coast, around 300 km for NCEP and 50 km for QuikSCAT (see Plate 11). The solution forced by NCEP differs from the one forced by QuikSCAT in a way that is consistent with the discussion above: nearshore poleward currents even near the surface; an offshore doming of the isotherms associated with Ekman pumping; and overall warmer temperatures close to shore. Standing eddies, EKE patterns, and eddy fluxes also differ significantly as evident when comparing Plates 2d and 9 or Plates 3d and 10. With NCEP, the EKE is much reduced nearshore and has its maximum displaced farther offshore (as the California Current itself). The greater stability of prograde currents (i.e., currents that have the coast on the right in the northern hemisphere when facing downstream) is a possible explanation for these differences in EKE. Eddy heat fluxes differ mainly 150 to 300 km offshore where the solution forced with NCEP develops subsurface fluxes that limit the doming of the isotherms.

It seems desirable to reduce the uncertainty in our knowledge of wind profiles; see Plate 11 for a sense of the spread in the case of the CCS. Given that winds in climate models tend to resemble NCEP, this would help determine the role of atmospheric forcing in the EBS warm bias.

6. CONCLUSIONS

Eastern boundary upwelling systems have been largely neglected by the large-scale modeling community because their role in the climate system or the global ocean is less prominent than that of other regions. There are, however, numerous indications that EBS exert some influence on the dynamics of their respective basins, either because they actively contribute to stratus formation over wide areas or because there are oceanic pathways (by advection or through waves) between the EBS and the oceanic basin interior. The role of mesoscale eddies in these climate system connections is far from well established. Upper-oceanic heat

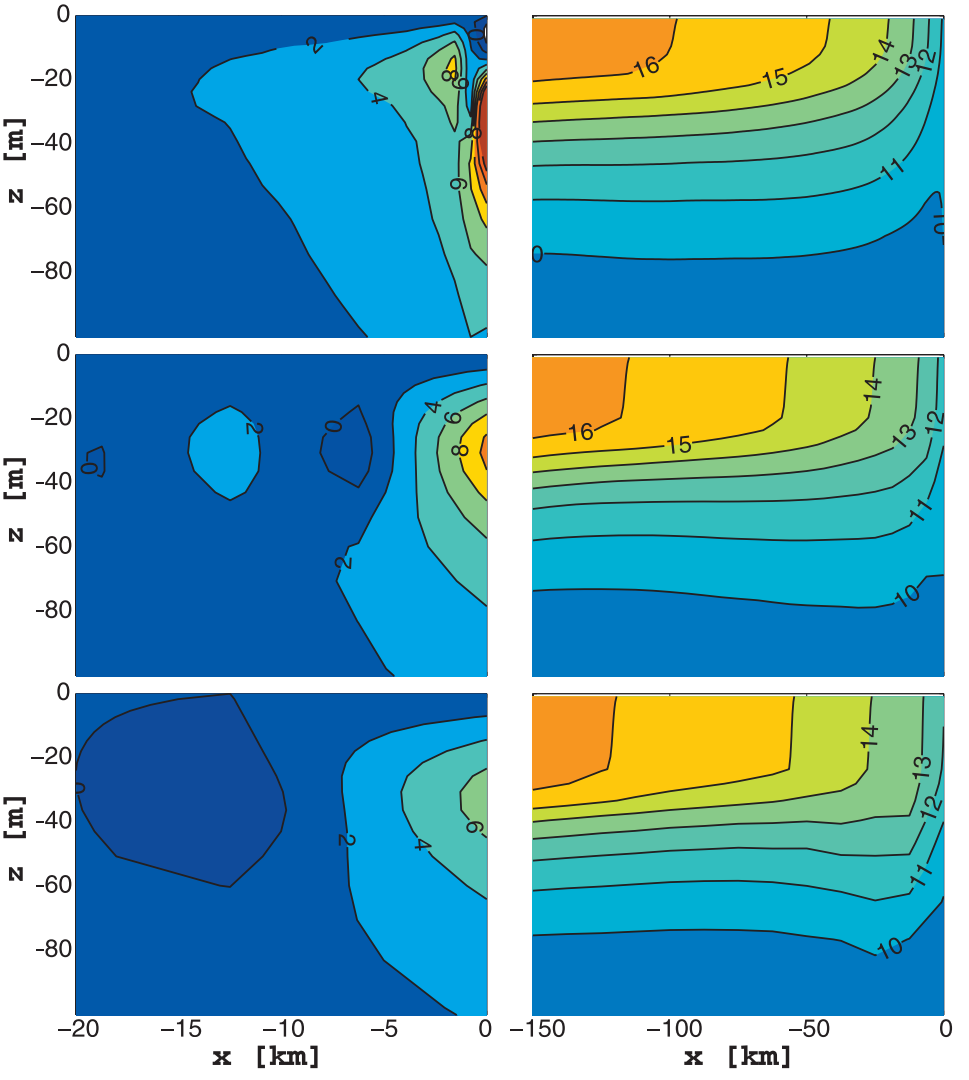

Plate 8. Cross-shore vertical sections of vertical velocity (left; m day^{-1}) and temperature (right; °C) in an idealized California Current System [*Capet et al.*, 2007a] at three different horizontal resolutions (dx = 0.75, 3, and 12 km, top to bottom). Both quantities are averaged alongshore over 600 km. Note the different scales in the cross-shore direction. At 0.75-km resolution, the vertical velocity at the shore reaches 50 m/day^{-1}.

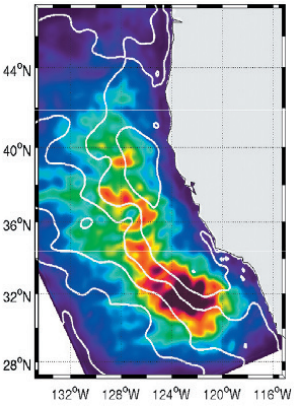

Plate 9. Same as Plate 2d but for a solution forced with NCEP climatological winds.

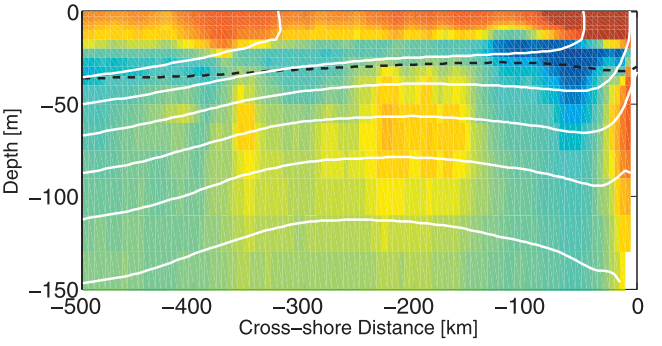

Plate 10. Same as Plate 3d but for a solution forced with NCEP climatological winds.

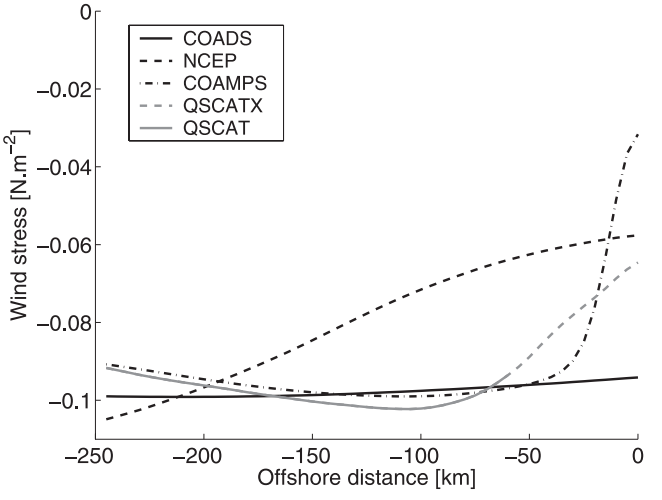

Plate 11. Spring-Summer climatological alongshore wind stress averaged between 34°N and 42°N in the CCS as a function of distance from the coast. COADS [*Da Silva et al.*, 1994], NCEP, COAMPS [*Kindle et al.*, 2002; *Pickett and Paduan*, 2003], and QuikSCAT are represented. Negative wind stress is equatorward. The climatologies are computed over the period 1999–2004, except for COADS (1945–1989). For QuikSCAT, both the actual data (solid gray line) and their near-shore linear extrapolation (dashed gray line) are shown.

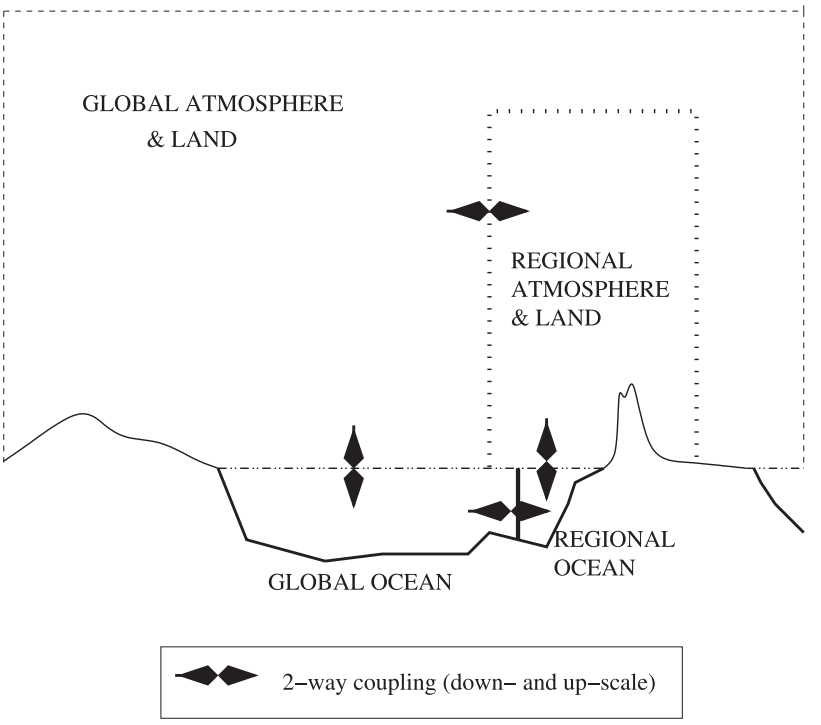

Figure 1. Schematic of an embedded (regional within global) coupled atmosphere-ocean model.

budgets carried out for the four major EBS indicate that eddy heat flux divergences are locally significant and may affect the atmospheric boundary layer functioning, hence also the stratus cloud deck formation [*Colbo and Weller*, 2008]. Explicitly resolving these eddy fluxes, and also better representing coastal processes with scales on the order of the first baroclinic deformation radius or less (coastal upwelling, coastal trapped waves), are the direct main benefits to expect from EBS eddy-resolving models. Indirectly, this may also improve the realism of OGCMs whose EBS biases are quite large at present. Nesting strategies between OGCMs and regional models are currently under development and should limit the computational cost of increasing the resolution for the EBS as well as in other oceanic regions of particular interest (Figure 1). The technical aspects of coupling between such a nested oceanic modeling system and its atmospheric counterpart make this a challenging path, but it would deliver an adequate framework to represent and understand EBS and other regional dynamics in their full complexity, including climate downscaling and upscaling effects as well as ocean-atmosphere feedbacks.

Acknowledgments. The altimeter products were produced by SSALTO/DUACS and distributed by Aviso, with support from CNES. Rio05 was produced by CLS Space Oceanography Division. Alexander Shchepetkin is acknowledged for his unshakable dedication to improving the physical and numerical aspects of ROMS. We acknowledge the Office of Naval Research for support under grant ONR N00014-04-1-0401 and the InterUp (LEFE-IDAO program) for travel support.

Notes

1. Among the various regional models, ROMS [*Shchepetkin and McWilliams*, 2008] is today often preferred when simulating EBS because of its weakly diffusive numerical schemes, a desirable feature given the importance of small-scale processes in upwelling systems.
2. As customary, EKE is defined as $1/2(u'^2 + v'^2)$ where u' and v' are velocity perturbations relative to a long-term time-mean. The bulk of EKE in the ocean is associated with scales around the first-baroclinic deformation radius [*Stammer*, 1997] that is with mesoscale variability, but also see Section 2.1 for a discussion on nearshore EBS regions. Note that EBS EKE estimates differ significantly depending on the type of observations they are based on [*Chereskin et al.*, 2000; *Kelly et al.*, 1998; *Ducet et al.*, 2000; *Pascual et al.*, 2006].
3. These results are expected to apply with the caveat that the intensity of the perturbations should be limited near a continental boundary.
4. Some caution is needed because circulation patterns with scales on the order of 100 km may not be adequately resolved in the Rio05 product

[*Rio and Hernandez*, 2004]. In particular, the standing eddies that are a conspicuous feature of the CCS and, to a lesser extent, the other EBS are nearly absent in Plate 1.

5. Bolus velocities arise from correlations between density (or isopycnal thickness) and velocity [*Gent et al.*, 1995]. In effect, they should be thought of as a mass transport due to eddies.
6. Using mesoscale-resolving solutions for the CCS, Nagai, et al. (Dominant role of eddies in offshore transports in the California Current System, submitted to *Journal of Geophysical Research*, 2007) show that eddy subduction at upper-oceanic fronts takes some of the upwelled nutrients away from the surface, and therefore, primary production tends to decrease when mesoscale activity is resolved.
7. Off Oregon, the scaling of Estrade et al. (submitted manuscript, 2007) for the cross-shore width of an upwelling cell D/s (where D is the Ekman depth and s the slope of the continental shelf) is on the order of 1 km.

REFERENCES

Barnier, B., L. Siefried, and P. Marchesiello (1995), Thermal forcing for a global ocean circulation model using a three-year climatology of ECMWF analyses., *J. Mar. Syst., 6*, 363–380.

Barth, J. (1994), Short wavelength instabilities on coastal jets and fronts, *J. Geophys. Res.*, *99*(C8), 16095–16115.

Batteen, M. (1997), Wind-forced modeling studies of currents, meanders and eddies in the California Current System, *J. Geophys. Res.*, *102*(C1), 985–1010.

Boccaletti, G., R. Ferrari, and B. Fox-Kemper (2007), Mixed layer instabilities and restratification, *J. Phys. Oceanogr.*, *37*, 2228–2250.

Bograd, S., and A. Mantyla (2005), On the subduction of upwelled waters in the California current, *J. Mar. Res.*, *63*, 863–885.

Boyer, T., and S. Levitus (1998), Objective analyses of temperature and salinity for the world ocean on a 1/4° grid. NOAA Atlas NESDIS, Washington, DC.

Brink, K., R. Beardsley, J. Paduan, R. Limeburner, M. Caruso, and J. Sires (2000), A view of the 1993–1994 California current based on surface drifters, floats, and remotely sensed data, *J. Geophys. Res.*, *105*(C4), 8575–8604.

Bryan, K., J. Dukowicz, and R. Smith (1999), On the mixing coefficient in the parameterization of bolus velocity, *J. Phys. Oceanogr.*, *29*, 2442–2456.

Capet, X. J., P. Marchesiello, and J. C. McWilliams (2004), Upwelling response to coastal wind profiles, *Geophys. Res. Lett.*, *31*, L13311.

Capet, X., J. McWilliams, M. Molemaker, and A. Shchepetkin (2008a), Mesoscale to submesoscale transition in the California Current System: Flow structure and eddy flux, *J. Phys. Oceanogr.*, in press.

Capet, X., J. McWilliams, M. Molemaker, and A. Shchepetkin (2008b), Mesoscale to submesoscale transition in the California Current System: Frontal processes, *J. Phys. Oceanogr.*, in press.

Castelao, R., and J. Barth (2007), The role of wind-stress curl in jet separation at a cape, *J. Phys. Oceanogr.*, *37*, 2652–2671.

Chaigneau, A., and O. Pizarro (2005), Mean surface circulation and mesoscale turbulent flow characteristics in the eastern South Pacific from satellite tracked drifters, *J. Geophys. Res.*, *110*, C05014, doi:10.1029/2004JC002628.

Chereskin, T., M. Morris, P. Niiler, P. Kosro, R. Smith, S. Ramp, C. Collins, and D. Musgrave (2000), Spatial and temporal characteristics of the mesoscale circulation of the California Current from eddy-resolving moored and shipboard measurements, *J. Geophys. Res.*, *105*(C1), 1245–1269.

Colbo, K., and R. Weller (2008), The variability and heat budget of the upper ocean under the Chile–Peru stratus, *J. Mar. Res.*, in press.

Collins, C. A., L. M. Ivanov, O. V. Melnichenko, and N. Garfield (2004), California Undercurrent variability and eddy transport estimated from RAFOS float observations, *J. Geophys. Res.*, *109*, C05028, doi:10.1029/2003JC002191.

Cornuelle, B., T. Chereskin, P. Niiler, M. Morris, and D. Musgrave (2000), Observations and modeling of a California undercurrent eddy, *J. Geophys. Res.*, *105*(C1), 1227–1243.

Da Silva, A., C. Young, and S. Levitus (1994), Atlas of surface marine data 1994, Vol. 1, Algorithms and procedures, *NOAA Atlas NESDIS*, *6*, 74 pp.

Ducet, N., P. Y. Le Traon, and G. Reverdin (2000), Global high-resolution mapping of ocean circulation from TOPEX/Poseidon and ERS-1 and -2, *J. Geophys. Res.*, *105*(C8), 19477–19498.

Durski, S., and J. Allen (2005), Finite-amplitude evolution of instabilities associated with the coastal upwelling front, *J. Phys. Oceanogr.*, *35*, 1606–1628.

Enriquez, A., and C. Friehe (1995), Effect of wind stress and wind stress curl variability on coastal upwelling, *J. Phys. Oceanogr.*, *25*, 1651–1671.

Fennel, W., and H. Laas (2006), On the impact of wind curls on coastal currents, *J. Mar. Sys.*, doi:10.1016/j.jmarsys.2006.11.004.

Florenchie, P., C. Reason, J. Lutjeharms, M. Rouault, R. C., and S. Masson (2004), Evolution of interannual warm and cold events in the Southeast Atlantic ocean, *J. Clim.*, *17*, 2318–2334.

Gammelsrod, T., C. Bartholomae, D. Boyer, V. Filipe, and M. O'Toole (1998), Intrusion of warm surface water along the Angolan-Namibian coast in February–March 1995: The 1995 Benguela Nino, *S. Afr. J. Mar. Sci.*, *19*, 41–56.

Garreaud, R., and R. Muñoz (2005), The low-level jet off the west coast of subtropical South America: structure and variability, *Mon. Weather Rev.*, *133*, 2203.

Gent, P., J. Willebrand, T. McDougall, and J. McWilliams (1995), Parameterizing eddy-induced tracer transports in ocean circulation models, *J. Phys. Oceanogr.*, *25*, 463–474.

Haine, T., and J. Marshall (1998), Gravitational, symmetric, and baroclinic instability of the ocean mixed layer, *J. Phys. Oceanogr.*, *28*, 634–658.

Haney, R., R. Hale, and D. Dietrich (2001), Offshore propagation of eddy kinetic energy in the California Current, *J. Geophys. Res.*, *106*(C6), 11709–11717.

Hormazabal, S., G. Shaffer, and O. Leth (2004), Coastal transition zone off Chile, *J. Geophys. Res.*, *109*, C01021, doi:10.1029/2003JC001956.

Hoskins, B. (1982), The mathematical theory of frontogenesis, *Annu. Rev. Fluid Mech.*, *14*, 131–151.

Ikeda, M., and W. Emery (1984), Satellite observations and mod-

eling of meanders in the California Current System off Oregon and Northern California, *J. Phys. Oceanogr.*, *14*, 1434–1449.

Ikeda, M., L. Mysak, and W. Emery (1984), Observations and modeling of satellite-sensed meanders and eddies off Vancouver Island, *J. Phys. Oceanogr.*, *14*, 3–21.

Kelly, K., R. Beardsley, R. Limeburner, K. Brink, J. Paduan, and T. Chereskin (1998), Variability of the near-surface eddy kinetic energy in the California Current based on altimetric, drifter, and moored current data, *J. Geophys. Res.*, *103*(C6), 13067–13083.

Kindle, J. C., R. M. Hodur, S. deRada, J. D. Paduan, L. K. Rosenfeld, and F. Q. Chavez (2002), A COAMPS™ reanalysis for the Eastern Pacific: Properties of the diurnal sea breeze along the central California coast, *Geophys. Res. Lett.*, *29*(24), 2203, doi:10.1029/2002GL015556.

Kosro, P., et al. (1991), The structure of the transition zone between coastal waters and the open ocean off northern California, Winter and Spring 1987, *J. Geophys. Res.*, *96*(C8), 14707–14730.

Lapeyre, G., P. Klein, and B. Hua (2007), Oceanic restratification forced by surface frontogenesis, *J. Phys. Oceanogr.*, *36*, 1577–1590.

Large, W., and G. Danabasoglu (2006), Attributions and impacts of upper-ocean biases in CCSM3, *J. Clim.*, *19*, 2325–2346.

Lazar, A., T. Inui, P. Malanotte-Rizzoli, A. J. Busalacchi, L. Wang, and R. Murtugudde (2002), Seasonality of the ventilation of the tropical Atlantic thermocline in an ocean general circulation model, *J. Geophys. Res.*, *107*(C8), 3104, doi:10.1029/2000JC000667.

Leth, O., and J. F. Middleton (2004), A mechanism for enhanced upwelling off central Chile: Eddy advection, *J. Geophys. Res.*, *109*, C12020, doi:10.1029/2003JC002129.

Marchesiello, P., and P. Estrade (2008), Eddy activity and mixing in upwelling systems: A comparative study of northwest Africa and California regions, *Int. J. Earth Sci.*, in press.

Marchesiello, P., J. McWilliams, and A. Shchepetkin (2003), Equilibrium structure and dynamics of the California Current System, *J. Phys. Oceanogr.*, pp. 753–783.

Mitchum, G., and A. Clarke (1986), The frictional nearshore response to forcing by synoptic scale winds, *J. Phys. Oceanogr.*, *16*, 934–946.

Murray, C., S. Morey, and J. O'Brien (2001), Interannual variability of upper ocean vorticity balances in the Gulf of Alaska, *J. Geophys. Res.*, *106*(B6), 4479–4491.

Pares-Sierra, A., W. White, and C.-K. Tai (1993), Wind-driven coastal generation of annual mesoscale eddy activity in the California Current, *J. Phys. Oceanogr.*, *23*, 1110–1121.

Pascual, A., Y. Faugère, G. Larnicol, and P.-Y. Le Traon (2006), Improved description of the ocean mesoscale variability by combining four satellite altimeters, *Geophys. Res. Lett.*, *33*, L02611, doi:10.1029/2005GL024633.

Pedlosky, J. (1978), A nonlinear model of the onset of upwelling, *J. Phys. Oceanogr.*, *8*, 178–187.

Pedlosky, J. (1987), *Geophysical Fluid Dynamics*, 710 pp., Springer, Berlin.

Penven, P., V. Echevin, J. Pasapera, F. Colas, and J. Tam (2005), Average circulation, seasonal cycle, and mesoscale dynamics of the Peru Current System: A modeling approach, *J. Geophys. Res.*, *110*, C10021 doi:10.1029/2005JC002945.

Perez-Rodriguez, P., J. Pelegri, and A. Marrero-Diaz (2001), Dynamical characteristics of the Cape Verde frontal zone, *Sci. Mar.*, *65*(suppl. 1), 241–250.

Philander, S., and J. Yoon (1982), Eastern boundary currents and coastal upwelling, *J. Phys. Oceanogr.*, *12*, 862–879.

Pickett, M. H., and J. D. Paduan (2003), Ekman transport and pumping in the California Current based on the U.S. Navy's high-resolution atmospheric model (COAMPS), *J. Geophys. Res.*, *108*(C10), 3327, doi:10.1029/2003JC001902.

Rio, M.-H., and F. Hernandez (2004), A mean dynamic topography computed over the world ocean from altimetry, in situ measurements, and a geoid model, *J. Geophys. Res.*, *109*, C12032, doi:10.1029/2003JC002226.

Roy, C., and C. Reason (2001), ENSO related modulation of coastal upwelling in the eastern Atlantic, *Prog. Oceanogr.*, *49*, 245–255.

Shannon, L. V., A. Boyd, G. Bundrit, and J. Taunton-Clark (1986), On the existence of an El Nino-type phenomenon in the Benguela system, *J. Mar. Syst.*, *44*, 495–520.

Shchepetkin, A., and J. McWilliams (2007), Computational kernel algorithms for fine-scale, multi-process, long-time oceanic simulations, in *Handbook of Numerical Analysis: Special Volume: Computational Methods for the Atmosphere and the Oceans*, edited by R. Temam and J. Tribbia, Elsevier, in press.

Spall, M. (2000), Generation of strong mesoscale eddies by weak ocean gyres, *J. Mar. Res.*, *58*, 97–116.

Stammer, D. (1997), Global characteristics of ocean variability estimated from regional TOPEX/POSEIDON altimeter measurements, *J. Phys. Oceanogr.*, *27*, 1743–1769.

Strub, P., and C. James (2002), The 1997-1998 oceanic El Nino signal along the southeast and northeast Pacific boundaries—An altimetric view, *Prog. Oceanogr.*, *54*, 439–458.

Vega, A., Y. du-Penhoat, B. Dewitte, and O. Pizarro (2003), Equatorial forcing of interannual Rossby waves in the eastern South Pacific, *Geophys. Res. Lett.*, *30*(5), 1197, doi:10.1029/2002GL015886.

White, W., and J. Saur (1981), A source of annual baroclinic waves in the eastern subtropical North Pacific, *J. Phys. Oceanogr.*, *11*, 1452–1462.

White, W., T. C.K., and J. DiMento (1990), Annual Rossby wave characteristics in the California current region from the GEOSAT exact repeat mission, *J. Phys. Oceanogr.*, *20*, 1297–1311.

Winant, C., D. Dorman, C. Friehe, and R. Beardsley (1988), The marine layer off Northern California: an example of supercritical channel flow, *J. Atmos. Sci.*, *45*, 3588–3605.

Capet, X. Instituto Oceanográfico, Universidade de São Paulo, Pca. do Oceanografico 191 - Cidade Universitaria, 05508900, Sao Paulo, SP, Brazil. (xcapet@io.usp.br)